Optics Communications 473 (2020) 125999

Contents lists available at ScienceDirect

Optics Communications

journal homepage: www.elsevier.com/locate/optcom

Trapping and releasing bidirectional rainbow at terahertz frequencies

Jie Xu [a,b,c,1], Qian Shen [b,d,1], Kai Yuan [d], Xiaohua Deng [b], Yun Shen [e], Hang Zhang [f], Chiaho Wu [f], Sanshui Xiao [c], Linfang Shen [f,*]

[a] College of Material Science and Engineering, Nanchang University, Nanchang 330031, China
[b] Institute of Space Science and Technology, Nanchang University, Nanchang 330031, China
[c] Department of Photonics Engineering, Technical University of Denmark, DK-2800 Kgs. Lyngby, Denmark
[d] School of Information Engineer, Nanchang University, Nanchang, 330031, China
[e] Department of Physics, Nanchang University, Nanchang 330031, China
[f] Department of Applied Physics, Zhejiang University of Technology, Hangzhou 310023, China

ARTICLE INFO

Keywords:
Slow waves
Rainbow trapping and releasing
FDTD method

ABSTRACT

Rainbow trapping arisen from slow light effect has been attracted lots of attention for the past two decades. However, until now only unidirectional rainbow trapping has been proposed, which relies on a complicated configuration or technique. Here we propose and investigate a metal–dielectric-semiconductor-dielectric-metal structure, where the semiconductor layer is applied with an external DC magnetic field. We show that in such a waveguide configuration there exist branches of dispersion curves showing slow-light bands at finite propagation constants. The positions of the slow-light bands can be tuned by varying the thickness of the semiconductor or the dielectric layers in the waveguide. By tapering the waveguide, we first demonstrate bidirectional rainbow trapping in such a simple waveguide configuration, and more importantly the trapped rainbow can be easily released by changing the external magnetic field.

1. Introduction

Surface magnetoplasmon (SMPs) are nonreciprocal surface plasmons that were sustained at the interface of a magnetized plasmonic material and a dielectric. SMPs can exhibit one-way propagation under certain conditions. Such one-way SMPs are physically similar to the chiral edge states based on the quantum-Hall effect [1]. In 2008, F. D. M. Haldane and S. Raghu predicted the possibility of one-way electromagnetic (EM) mode in photonic crystals (PhCs) made of magnetic-optical (MO) materials [2]. Later, Wang and his colleagues experimentally demonstrated the one-way EM mode in the PhC made of gyromagnetic yttrium-iron-garnet (YIG) in microwave regime [3]. As an alternative form of one-way EM mode, one-way SMP was soon proposed as well, and due to the simple configuration, it draws more and more attentions recently [4–7].

The manipulation of EM wave or light is very attractive in both physics and technology. Particularly, slowing light is an interesting and meaningful issue due to its potential applications in energy storage [8–10], nonlinearity enhancement [11–13] and quantum optics [14,15]. At the very beginning, scientists studied the slow-light by using electromagnetically induced transparency (EIT), which is appropriate for fundamental investigations. However, that method is not applicable for practical applications [16,17]. In the past decade, many researchers were trying to slow light in PCs by introducing defects and photonic bandgap (PBG) [11,18–20]. Alternatively, some others preferred to utilize metamaterials [8]. Recently, we proposed a simple tapered metal–dielectric-semiconductor-metal (MDSM) structure in terahertz regime [21]. It was shown that this MDSM structure is capable to slow wave (SMP) and to trap 'rainbow'.

In this paper, we further propose an improved model, which is a metal–dielectric-semiconductor-dielectric-metal (MDSDM) structure. The propagation properties of SMPs in this MDSDM structure are studied theoretically. It is shown that the dispersion property of SMPs in the MDSDM structure could be tailored by varying the thickness of the dielectric or semiconductor layers. Furthermore, we propose a tapered MDSDM structure, and show that bidirectional slow waves, rainbow trapping and its releasing can be realized in this structure by using the COMSOL and the finite-difference time-domain (FDTD) method.

2. Physical model and dispersion property

The proposed MDSDM waveguide is illustrated in Fig. 1(a), and its dispersion property is investigated at first. In the terahertz regime, the metal in the waveguide can be approximated as perfect electric conductor (PEC) [22]. The semiconductor is gyroelectric anisotropic

* Corresponding author.
E-mail address: lfshen@zjut.edu.cn (L. Shen).
[1] These authors contributed equally to this work.

https://doi.org/10.1016/j.optcom.2020.125999
Received 30 November 2019; Received in revised form 28 March 2020; Accepted 19 April 2020
Available online 25 April 2020

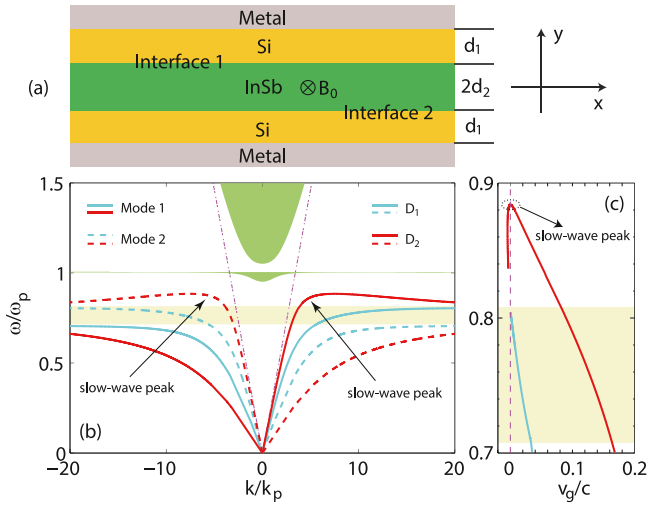

Fig. 1. (a) The schematic of the MDSDM structure. (b) The dispersion curves of SMPs for the cases of $D_1 = (0.025\lambda_p, 0.025\lambda_p)$ (red lines) and $D_2 = (0.025\lambda_p, 0.006\lambda_p)$ (cyan lines). The solid and dashed lines correspond to the modes 1 and 2 of SMPs, respectively. (c) The group velocity (v_g) versus frequency for the higher dispersion branch of mode 1. The yellow shaded area indicates the frequency region between the different asymptotic frequencies. The green shaded areas represent the bulk-mode zones in the semiconductor. The other parameters are as follows: $\varepsilon_r = 11.68$, $\varepsilon_\infty = 15.6$, $\nu = 0$, and $\omega_c = 0.1\omega_p$. (For interpretation of the references to color in this figure legend, the reader is referred to the web version of this article.)

under the external DC magnetic field (B_0), and its relative permittivity has the form of [23]:

$$\vec{\varepsilon} = \varepsilon_\infty \begin{bmatrix} \varepsilon_1 & -i\varepsilon_2 & 0 \\ i\varepsilon_2 & \varepsilon_1 & 0 \\ 0 & 0 & \varepsilon_3 \end{bmatrix}, \tag{1}$$

with

$$\varepsilon_1 = 1 - \frac{(\omega + i\nu)\omega_p^2}{\omega\left[(\omega + i\nu)^2 - \omega_c^2\right]}$$

$$\varepsilon_2 = \frac{\omega_c\omega_p^2}{\omega\left[(\omega + i\nu)^2 - \omega_c^2\right]}$$

$$\varepsilon_3 = 1 - \frac{\omega_p^2}{\omega(\omega + i\nu)}$$

where ω is the angular frequency of wave, ω_p and $\omega_c = eB_0/m^*$ (m^* is the effective mass of electron) are the plasma and electron cyclotron frequencies in the semiconductor, respectively; ε_∞ is the high-frequency (relative) permittivity of the semiconductor, and ν is the electron scattering frequency. To distinguish the propagating mode from the evanescent one, we will take the (material) loss parameter $\nu = 0$ in analyzing the dispersion for the MDSDM waveguide. In the later simulations, nonzero value of ν will be taken into account, and it will be shown that the propagation property in the lossy case is in good agreement with the dispersion diagram. In this paper, the semiconductor is assumed to be InSb with $\varepsilon_\infty = 15.6$ and $\omega_p = 4\pi \times 10^{12}$ rad/s [24], and the dielectric is the silicon (Si) with the relative permittivity $\varepsilon_r = 11.68$ [5].

As in the case of the single dielectric-semiconductor interface, SMPs in the MDSDM waveguide have modal fields that are transverse-magnetic-polarized. From the Maxwell's equations and the boundary conditions, the dispersion relation of SMPs in the MDSDM structure can be derived, which is given by

$$\frac{2\varepsilon_\nu\alpha_1}{\varepsilon_r}\tanh(\alpha_1 d_1) + \frac{F}{\alpha}\tanh(2\alpha d_2) = 0, \tag{2}$$

with

$$F = \left(\frac{2\varepsilon_\nu\alpha_1}{\varepsilon_r}\tanh(\alpha_1 d_1)\right)^2 - \left(\frac{\varepsilon_2}{\varepsilon_1}k\right)^2 + \alpha^2,$$

where k is the propagation constant; ε_r is the relative permittivity of the dielectric, $\varepsilon_\nu = \varepsilon_1 - \varepsilon_2^2/\varepsilon_1$ being the Voigt permittivity; $\alpha = \sqrt{k^2 - \varepsilon_\nu k_0^2}$ and $\alpha_1 = \sqrt{k^2 - \varepsilon_r k_0^2}$, being the attenuation coefficients in the semiconductor and dielectric layers, respectively. The SMP modes in the MDSDM structure are numerically calculated with Eq. (2), and there exist two types of SMP modes, whose fields peak at the upper and lower interfaces, which are labeled by interfaces 1 and 2 in Fig. 1(a), respectively. Evidently, the two modes are mainly supported by interface 1 or interface 2, and we refer to them as mode 1 and mode 2, respectively. The dispersion curves for modes 1 and 2 are symmetrical with respective to $k = 0$. For each mode, there are two different asymptotic frequencies, at which $k \to \pm\infty$. From Eq. (2), the asymptotic frequencies $\omega_{sp}^{(1)}$ and $\omega_{sp}^{(2)}$ are found to be

$$\omega_{sp}^{(1)} = \frac{1}{2}\left(\sqrt{\omega_c^2 + 4\frac{\varepsilon_\infty}{\varepsilon_\infty + \varepsilon_r}\omega_p^2} + \omega_c\right), \tag{3a}$$

$$\omega_{sp}^{(2)} = \frac{1}{2}\left(\sqrt{\omega_c^2 + 4\frac{\varepsilon_\infty}{\varepsilon_\infty + \varepsilon_r}\omega_p^2} - \omega_c\right). \tag{3b}$$

For mode 1, the right dispersion branch with $k > 0$ is higher with the asymptotic frequency $\omega_{sp}^{(1)}$, and the left dispersion branch with $k < 0$ is lower with the asymptotic frequency $\omega_{sp}^{(2)}$. The situation is opposite for mode 2.

A waveguide parameter of $D = (d_1, d_2)$ was introduced for convenience. Fig. 1(b) shows the dispersion curves for the SMPs for the cases $D_1 = (0.025\lambda_p, 0.025\lambda_p)$ (the cyan lines) and $D_2 = (0.025\lambda_p, 0.006\lambda_p)$ (the red lines), where $\lambda_p = 2\pi c/\omega_p$, and c is the light speed in vacuum. The shaded yellow area represents the (frequency) region between the two asymptotic frequencies. In the D_1 case, there is no SMP mode above this region. In contrast, in the D_2 case, where the semiconductor is thinner (than that for the D_1 case), the higher branches of dispersion curves peak at finite k above that region, and hence SMPs are slow waves around the peak points for both modes. Evidently, these slow-wave peaks result from the coupling between SMPs sustained by the two InSb-Si interfaces in the waveguide. As there is no SMP mode above the slow-wave peak, the peak point determines the cutoff frequency, which is quite different from that in our previous work [21]. In the previous work, it is the lower branch with $\omega_{sp}^{(2)}$ peaks at finite k, so there is still SMP mode above the slow-wave peak. The reason for this phenomenon should be that there is only one Si-InSb interface in the previous asymmetric waveguide. For the present symmetric waveguide, the group velocity (v_g) on the higher branch of mode 1 is plotted in Fig. 1(c) for the D_2 case. Evidently, v_g vanishes at the vertex of the slow-wave peak. From Fig. 1(b), it is clear that v_g is always positive for finite positive k in the D_1 case, and $v_g \to 0$ only as $k \to \infty$.

The relation between the slow-wave peak and the waveguide parameter D is illustrated detailedly in Fig. 2. The higher dispersion branches for the two modes are plotted in Fig. 2(a) for the four different D cases, where $d_1 + d_2 = 0.031\lambda_p$ is kept. The four case are as follows: $D_2 = (0.025\lambda_p, 0.006\lambda_p)$, $D_3 = (0.03\lambda_p, 0.001\lambda_p)$, $D_4 = (0.015\lambda_p, 0.016\lambda_p)$, and $D_5 = (0.01\lambda_p, 0.021\lambda_p)$. As seen in Fig. 2(a), the slow-wave peaks occur in the D_2 and D_3 cases, and the corresponding cutoff frequencies ω_{cf}, at which $v_g = 0$, are different. It is found that ω_{cf} increases with d_1 and decreases with d_2. In Fig. 2(b) the relation between ω_{cf} and $D = (d_1, d_2)$ is further revealed in the ultra thin waveguide condition ($d_1, d_2 \sim 10^{-2}\lambda_p$). The white dashed line represents the dividing line of $\omega_{cf} = \omega_{sp}^{(1)}$. On the left side, $\omega_{cf} > \omega_{sp}^{(1)}$, and on the right side, $\omega_{cf} < \omega_{sp}^{(1)}$. Obviously, both d_1 and d_2 can affect ω_{cf}, and either increasing d_1 or decreasing d_2 lead to increasing ω_{cf}.

3. Bidirectional rainbow trapping and releasing

Fig. 2 shows that the cutoff frequency of SMPs varies with the waveguide parameter D. It implies a possible way to achieve bidirectional rainbow trapping, which has never been reported before. For this purpose, a MDSDM structure consisting of two tapered sections and

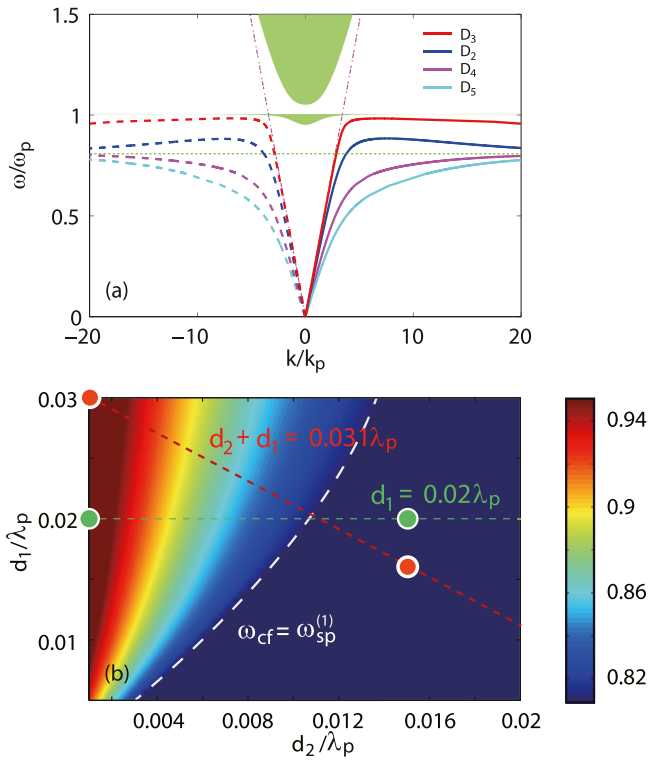

Fig. 2. (a) The higher dispersion branches of SMP modes for different D cases. The solid and dashed lines correspond to modes 1 and 2, respectively. The dash-dotted lines represent the light lines in Si, and the dotted line indicates the frequency of $\omega_{sp}^{(1)}$. (b) The cutoff frequency ω_{cf} as a function of D. The white dashed line represents the dividing line, at which $\omega_{cf} = \omega_{sp}^{(1)}$. The four cases in (a) are $D_2 = (0.025\lambda_p, 0.006\lambda_p)$, $D_3 = (0.03\lambda_p, 0.001\lambda_p)$, $D_4 = (0.015\lambda_p, 0.016\lambda_p)$, and $D_5 = (0.01\lambda_p, 0.021\lambda_p)$. The other parameters are the same as in Fig. 1. (For interpretation of the references to color in this figure legend, the reader is referred to the web version of this article.)

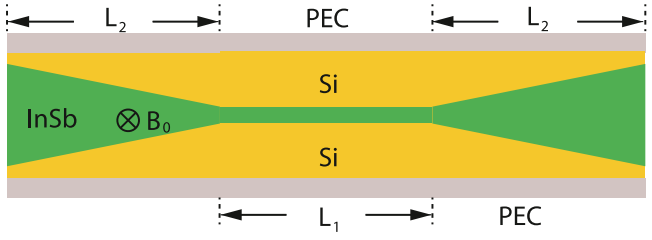

Fig. 3. The schematic of the structure for bidirectional rainbow trapping. The total thickness of the Si and InSb is kept constant along the whole structure. $L_1 = L_2 = 100$ μm.

one uniform section is designed, as illustrated in Fig. 3. The length of the uniform part is L_1 and the two tapered parts have the same length of L_2. The geometric parameter is $D_1 = (0.03\lambda_p, 0.001\lambda_p)$ for the uniform part and $D_2 = (0.016\lambda_p, 0.015\lambda_p)$ at the structure ends. Note that $d_1 + d_2 = 0.031\lambda_p$ is kept along the tapered parts, which is marked by the red dashed line in Fig. 2(b). The upper red point on that line corresponds to the case of D_1, and the lower one corresponds to the case of D_2. Our numerical calculation shows that ω_{cf} is $0.98\omega_p$ (the largest value on the red line) for the uniform waveguide, and it is $0.81\omega_p$ ($= \omega_{sp}^{(1)}$) at the structure ends. Thus, the local cutoff frequency in this structure varies in the range from $0.81\omega_p$ to $0.98\omega_p$.

The full-wave simulations was performed in the loss case of $\nu = 0.001\omega_p$ by using the commercial software COMSOL. Fig. 4 shows the electric field distributions at four different operating frequencies, i.e., (a) $\omega = 0.82\omega_p$, (b) $\omega = 0.85\omega_p$, (c) $\omega = 0.88\omega_p$, and (d) $\omega = 0.94\omega_p$. As expected, once a magnetic current source is placed in the middle of

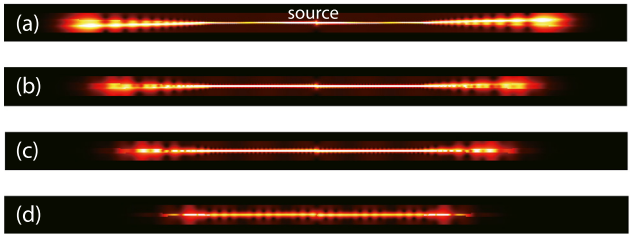

Fig. 4. The electric field distributions in the tapered structure for different frequencies. (a) $0.82\omega_p$, (b) $0.85\omega_p$, (c) $0.88\omega_p$, and (d) $0.94\omega_p$. For all cases, $\omega_c = 0.1\omega_p$ and $\nu = 0.001\omega_p$.

the designed structure, clear bidirectional rainbow trapping is observed in it, and the wave with higher frequency ($\omega > \omega_{sp}^{(1)}$) is trapped at the thinner InSb position. The result shows that the designed waveguide is capable to trap waves for the frequencies in the range $[0.81\omega_p, 0.98\omega_p]$.

Another important function of the designed waveguide is the capability of releasing the trapped wave. The optical property of MO material could be tuned by changing the external magnetic field. In Fig. 5(a), the asymptotic frequencies and cutoff frequency ω_{cf} are plotted as the functions of ω_c for $D = (0.03\lambda_p, 0.001\lambda_p)$. The green and yellow shaded zones correspond to the regions for $\omega_{\rm sp}^{(1)} < \omega < \omega_{cf}$ and $\omega_{\rm sp}^{(2)} < \omega < \omega_{\rm sp}^{(1)}$, respectively. For convenience, the two zones are named as the trapping zone and releasing zone, respectively. The four points in the trapping zone correspond to the four working frequencies in Fig. 4. Nevertheless, once the external magnetic field is increased to $\omega_c = 0.4\omega_p$, all of the four frequencies fall into the releasing zone (see the right four points). The SMPs lie in the releasing zone can always propagate along the InSb-Si interfaces since $|v_g| > 0$, i.e., the SMPs can not be trapped again in the waveguide. The simulation was performed for an example, whose result is shown in the inset of Fig. 5(a). In that simulation, $\omega_c = 0.4\omega_p$ and $\omega = 0.94\omega_p$. It is obvious that the SMPs excited by the source can propagate to the structure end, instead of being trapped. Additionally, different structure for rainbow trapping and releasing can also be designed based on the present theory. An example is illustrated in Fig. 5(b)–(d). In this structure, the total thickness of the Si and InSb layers varies in the tapered parts, but the thickness of the Si layers is kept constant [$d_1 = 0.02\lambda_p$, corresponding to the horizontal green line in Fig. 2(b)]. The bidirectional rainbow trapping can also be achieved, as shown in Fig. 5(c), where $\omega_c = 0.1\omega_p$ and only one frequency is presented, which is $\omega = 0.94\omega_p$. Fig. 5(d) shows the wave releasing when $\omega_c = 0.4\omega_p$.

To get insight into the process of trapping and releasing wave, additional simulations were performed by using the FDTD method. For the semiconductor, the simulation equations in time domain can be written as follows

$$\frac{\partial j_x^{\pm}}{\partial t} + 2\pi(\overline{\nu} \mp i\overline{\omega}_c) j_x^{\pm} = 2\pi^2 \varepsilon_\infty e_x, \tag{4a}$$

$$\frac{\partial j_y^{\pm}}{\partial t} + 2\pi(\overline{\nu} \mp i\overline{\omega}_c) j_y^{\pm} = 2\pi^2 \varepsilon_\infty e_y, \tag{4b}$$

$$\frac{\partial h_z}{\partial y} = \varepsilon_\infty \frac{\partial e_x}{\partial t} + (j_x^{+} + j_x^{-}) - i(j_y^{+} - j_y^{-}), \tag{4c}$$

$$-\frac{\partial h_z}{\partial x} = \varepsilon_\infty \frac{\partial e_y}{\partial t} + (j_y^{+} + j_y^{-}) + i(j_x^{+} - j_x^{-}), \tag{4d}$$

$$\frac{\partial e_y}{\partial x} - \frac{\partial e_x}{\partial y} = -\frac{\partial h_z}{\partial t}, \tag{4e}$$

where $\overline{\omega}_c = \omega_c/\omega_p$, and $\overline{\nu} = \nu/\omega_p$; $j_x^{\pm}$ and $j_y^{\pm}$ represent the effective electric current components. In Eq. (4), the spatial variables are normalized by λ_p and the time variable by $T_p = 2\pi/\omega_p$. e_x, e_y, and h_z are the normalized EM field components, i.e., $e_{x,y} = \sqrt{\varepsilon_0} E_{x,y}$, $h_z = \sqrt{\mu_0} H_z$. For the Si layer, $j_x^{\pm} = 0$ and $j_y^{\pm} = 0$, thus the simulation equations are simplified to

$$\frac{\partial h_z}{\partial y} = \varepsilon_r \frac{\partial e_x}{\partial t}, \tag{5a}$$

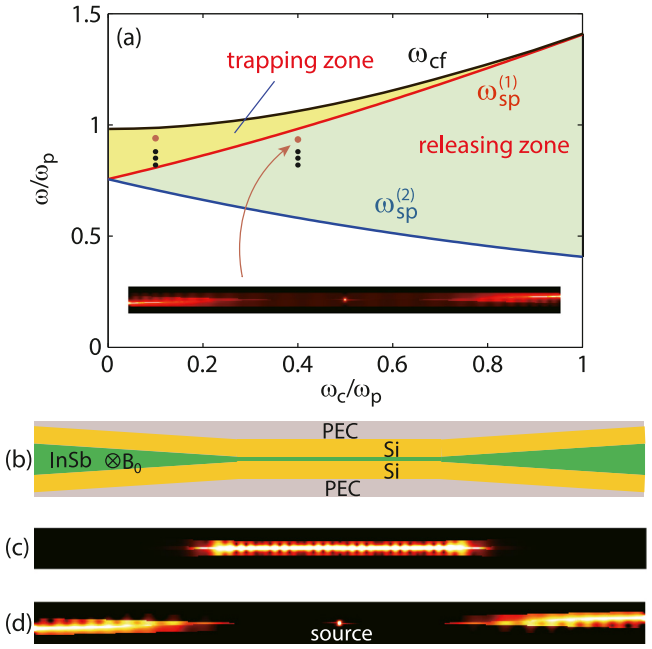

Fig. 5. (a) ω_{cf}, $\omega_{sp}^{(1)}$, and $\omega_{sp}^{(2)}$ as functions of ω_c for the uniform waveguide with $D = (0.03\lambda_p, 0.001\lambda_p)$. The upper and lower shaded areas represent the trapping and releasing zones in a tapered structure. The four points in the trapping zone correspond to the four cases in Fig. 4. The inset shows the electric field distribution in the first tapered structure for $\omega_c = 0.4\omega_p$ and $\omega = 0.94\omega_p$. (b) The schematic of the second tapered structure for bidirectional rainbow trapping and releasing. The thickness of the Si layers is kept to be $d_1 = 0.02\lambda_p$. (c),(d) The electric field distributions in the second tapered structure for $\omega_c = 0.1\omega_p$ and $0.4\omega_p$, respectively. The operation frequency in (c) and (d) is $\omega = 0.94\omega_p$. (For interpretation of the references to color in this figure legend, the reader is referred to the web version of this article.)

$$-\frac{\partial h_z}{\partial x} = \epsilon_r \frac{\partial e_y}{\partial t}, \tag{5b}$$

$$\frac{\partial e_y}{\partial x} - \frac{\partial e_x}{\partial y} = -\frac{\partial h_z}{\partial t}. \tag{5c}$$

The quantities $(e_x, e_y, h_z, j_x^{\pm}, j_y^{\pm})$ can be sampled in time and space domains as shown in Fig. 6(a,b). One of the challenges in applying the FDTD method in the MDSDM structure is how to define some material boundaries, i.e., the InSb-Si interfaces in the tapered parts. In the present simulations, zig-zag interfaces [see the upper panel in Fig. 6(c)] were employed instead of the original smooth interfaces [the blue dashed lines in Fig. 6(c)] in the real situation. In order to ensure the zig-zag interfaces are equivalent to the original ones, it is necessary to make the spatial steps (dx and dy) far less than the effective wavelength and the penetration depths (in the Si and semiconductor) of SMPs. The computation domain for the structure in Fig. 3 is discretized appropriately, as shown in Fig. 6(c), where only the straight-tapered joint region is displayed, and the time discretization is shown in Fig. 6(a). The FDTD simulations were performed with Eqs. (4) and (5), and the obtained results are shown in Fig. 7. Fig. 7(a)–(d) display the electric field distributions at the evolution times of $t = 5T_p$, $200T_p$, $300T_p$, and $t = 1000T_p$, respectively. Note that $\omega_c = 0.1\omega_p$ for $t \leq 200T_p$. As seen in Fig. 7(a,b), the EM energy is definitely trapped in the waveguide, which agrees well with the results shown in Fig. 4(d), which was obtained from the frequency-domain solution. When $t > 200T_p$, $\omega_c = 0.4\omega_p$ was set instead of $\omega_c = 0.1\omega_p$. Fig. 7(c) shows that the EM energy is no longer trapped. Instead, the energy is being released gradually. When $t = 1000T_p$, the EM energy is localized near the structure ends, for which the PEC boundary condition was applied. The results at this time is almost identical to those shown in the inset of Fig. 5(a). The rainbow trapping and releasing we numerically demonstrated are instructive for designing some functional devices.

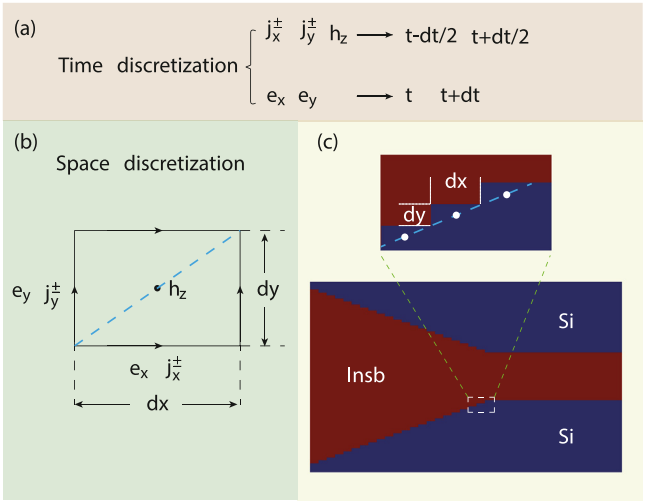

Fig. 6. The scheme of the FDTD simulation for a tapered structure. (a) Sampling points in time. (b) Sampling points in space. (c) The treatment of material boundaries. The blue dashed line in the upper panel represent the InSb-Si interface. (For interpretation of the references to color in this figure legend, the reader is referred to the web version of this article.)

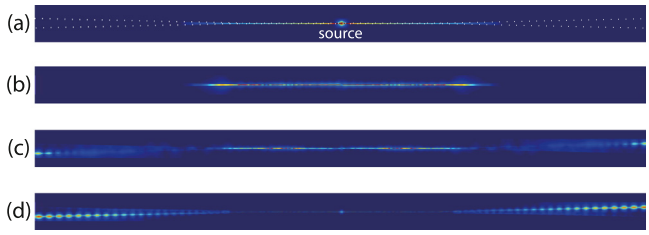

Fig. 7. The electric field distributions from the FDTD simulation at different evolution times. (a) $5T_p$, (b) $200T_p$, (c) $300T_p$, and (d) $1000T_p$. The value of ω_c is set at $0.1\omega_p$ for $t \leq 200T_p$), and it is changed to $0.4\omega_p$ for $t > 200T_p$. The other parameters are the same as in Fig. 4(d).

4. Conclusion

In this paper, a metal–dielectric-semiconductor-dielectric-metal (MDSDM) structure with an applied external DC magnetic field has been proposed and studied theoretically. For such a guiding structure, the dispersion curves have slow-wave peaks at terahertz frequencies. The cutoff frequency for the waveguide is just determined by the peak points. By varying the thickness of the semiconductor or the dielectric layers, the slow-wave peak can be effectively tuned. Therefore, waves can be manipulated by tapering the waveguide. Two tapered MDSDM structures have been proposed, in which rainbow trapping can be achieved bidirectionally. More importantly, the trapped rainbow can be well released by increasing the external magnetic field. These phenomena have been numerically demonstrated by both the frequency-domain (with the software COMSOL) and FDTD simulations. The proposed approach for trapping and releasing rainbow has promising applications in optical isolator, optical buffer, optical switch and other optical functional devices in optical integrated circuit.

Declaration of competing interest

The authors declare that they have no known competing financial interests or personal relationships that could have appeared to influence the work reported in this paper.

Acknowledgments

We acknowledge support by National Natural Science Foundation of China (NSFC) (61372005), National Natural Science Foundation of China (NSFC) under a key project (41331070), and Independent Research Fund Denmark (9041-00333B).

References

[1] R.E. Prange, S.M. Girvin, The Quantum Hall Effect, Springer, 1987, http://dx.doi.org/10.1007/978-1-4684-0499-9.
[2] F.D.M. Haldane, S. Raghu, Possible realization of directional optical waveguides in photonic crystals with broken time-reversal symmetry, Phys. Rev. Lett. 100 (1) (2008) 013904, http://dx.doi.org/10.1103/PhysRevLett.100.013904.
[3] Z. Wang, Y. Chong, J.D. Joannopoulos, M. Soljačić, Observation of unidirectional backscattering-immune topological electromagnetic states, Nature 461 (7265) (2009) 772, http://dx.doi.org/10.1038/nature08293.
[4] W. Qiu, Z. Wang, M. Soljačić, Broadband circulators based on directional coupling of one-way waveguides, Opt. Express 19 (22) (2011) 22248–22257, http://dx.doi.org/10.1364/OE.19.022248.
[5] L. Shen, Y. You, Z. Wang, X. Deng, Backscattering-immune one-way surface magnetoplasmons at terahertz frequencies, Opt. Express 23 (2) (2015) 950–962, http://dx.doi.org/10.1364/OE.23.000950.
[6] D. Jin, L. Lu, Z. Wang, C. Fang, J.D. Joannopoulos, M. Soljačić, L. Fu, N.X. Fang, Topological magnetoplasmon, Nature Commun. 7 (2016) 13486, http://dx.doi.org/10.1038/ncomms13486.
[7] K. Liu, A. Torki, S. He, One-way surface magnetoplasmon cavity and its application for nonreciprocal devices, Opt. Lett. 41 (4) (2016) 800–803, http://dx.doi.org/10.1364/OL.41.000800.
[8] K.L. Tsakmakidis, A.D. Boardman, O. Hess, 'Trapped rainbow' storage of light in metamaterials, Nature 450 (7168) (2007) 397, http://dx.doi.org/10.1038/nature06285.
[9] Y. Su, F. Liu, Q. Li, Z. Zhang, M. Qiu, System performance of slow-light buffering and storage in silicon nano-waveguide, in: Optical Transmission, Switching, and Subsystems V, Vol. 6783, 2007, p. 67832P, http://dx.doi.org/10.1117/12.743020.
[10] S.-W. Su, Y.-H. Chen, S.-C. Gou, T.-L. Horng, A.Y. Ite, Dynamics of slow light and light storage in a doppler-broadened electromagnetically-induced-transparency medium: A numerical approach, Phys. Rev. A 83 (1) (2011) 013827, http://dx.doi.org/10.1103/PhysRevA.83.013827.
[11] M. Soljačić, S.G. Johnson, S. Fan, M. Ibanescu, E. Ippen, J. Joannopoulos, Photonic-crystal slow-light enhancement of nonlinear phase sensitivity, J. Opt. Soc. Amer. B 19 (9) (2002) 2052–2059, http://dx.doi.org/10.1364/JOSAB.19.002052.
[12] J.E. Heebner, R.W. Boyd, Q.-H. Park, Slow light, induced dispersion, enhanced nonlinearity, and optical solitons in a resonator-array waveguide, Phys. Rev. E 65 (3) (2002) 036619, http://dx.doi.org/10.1103/PhysRevE.65.036619.
[13] Y. Chen, S. Blair, Nonlinearity enhancement in finite coupled-resonator slow-light waveguides, Opt. Express 12 (15) (2004) 3353–3366, http://dx.doi.org/10.1364/OPEX.12.003353.
[14] P.-C. Ku, F. Sedgwick, C.J. Chang-Hasnain, P. Palinginis, T. Li, H. Wang, S.-W. Chang, S.-L. Chuang, Slow light in semiconductor quantum wells, Opt. Lett. 29 (19) (2004) 2291–2293, http://dx.doi.org/10.1364/OL.29.002291.
[15] B. Wu, J.F. Hulbert, E.J. Lunt, K. Hurd, A.R. Hawkins, H. Schmidt, Slow light on a chip via atomic quantum state control, Nature Photonics 4 (11) (2010) 776, http://dx.doi.org/10.1038/nphoton.2010.211.
[16] T.F. Krauss, Why do we need slow light? Nature Photonics 2 (8) (2008) 448, http://dx.doi.org/10.1038/nphoton.2008.139.
[17] Z. Dutton, M. Budde, C. Slowe, L.V. Hau, Observation of quantum shock waves created with ultra-compressed slow light pulses in a bose-einstein condensate, Science 293 (5530) (2001) 663–668, http://dx.doi.org/10.1126/science.1062527.
[18] T. Baba, Slow light in photonic crystals, Nature photonics 2 (8) (2008) 465, http://dx.doi.org/10.1038/nphoton.2008.146.
[19] T.F. Krauss, Slow light in photonic crystal waveguides, J. Phys. D: Appl. Phys. 40 (9) (2007) 2666, http://dx.doi.org/10.1088/0022-3727/40/9/S07.
[20] A. Hosseini, X. Xu, D.N. Kwong, H. Subbaraman, W. Jiang, R.T. Chen, On the role of evanescent modes and group index tapering in slow light photonic crystal waveguide coupling efficiency, Appl. Phys. Lett. 98 (3) (2011) 031107, http://dx.doi.org/10.1063/1.3548557.
[21] J. Xu, S. Xiao, C. Wu, H. Zhang, X. Deng, L. Shen, Broadband one-way propagation and rainbow trapping of terahertz radiations, Opt. Express 27 (8) (2019) 10659–10669, http://dx.doi.org/10.1364/OE.27.010659.
[22] L. Shen, J. Xu, Y. You, K. Yuan, X. Deng, One-way electromagnetic mode guided by the mechanism of total internal reflection, IEEE Photonics Technol. Lett. 30 (2) (2017) 133–136, http://dx.doi.org/10.1109/LPT.2017.2776106.
[23] J. Brion, R. Wallis, A. Hartstein, E. Burstein, Theory of surface magnetoplasmons in semiconductors, Phys. Rev. Lett. 28 (22) (1972) 1455, http://dx.doi.org/10.1103/PhysRevLett.28.1455.
[24] T.H. isaac, W.L. Barnes, E. Hendry, Determining the terahertz optical properties of subwavelength films using semiconductor surface plasmons, Appl. Phys. Lett. 93 (24) (2008) 43–45, http://dx.doi.org/10.1063/1.3049350.